Evaluation of MIMO Antenna Configurations for High Data-Rate Systems / Original Article

Researcher Ammar Abdulimam Abbood

Islamic Azad University, Islamic Republic of Iran
e-mail: amareng1981@gmail.com

تقييم تكوينات هوائيات MIMO لانظمة ذات معدلات نقل بيانات عالية

الباحث عمار عبد الامام عبود

رئيس مهندسين، جامعة آزاد الإسلامية، جمهورية إيران الإسلامية

Abstract:

This paper introduces a new design of cat-shaped antenna in super wideband (SWB) and high data-rate multiple input multiple output (MIMO) systems. The single-element SWB antenna has a wide frequency range of 2.23 GHz up to more than 100 GHz with outstanding bandwidth ratio (BW Ratio = 44.84:1), fractional bandwidth (FBW = 191%), bandwidth dimensional ratio (BDR = 5567) and a peak gain of 9.52 dB.

The single antenna was also expanded to 22× MIMO array to further improve performance on multipath environments. Measurements and simulation show very good results using radiation patterns, isolation, channel capacity loss (CCL), envelope correlation coefficient (ECC), and total active reflection coefficient (TARC). The findings affirm the fact that the proposed antenna is quite applicable in portable UWB devices, 5G communication, and multi-band systems in S, C, X, Ku, K, Ka, V, and W bands.

Keywords: Super wideband antenna, MIMO, radiation efficiency, antenna isolation, 5G, compact antenna design.

المستخلص

يستعرض هذا البحث تصميم وتقييم هوائي جديد على شكل قطة لتطبيقات النطاق فائق الاتساع (SWB) وأنظمة MIMO عالية السرعة. يعمل الهوائي أحادي العنصر على نطاق ترددي واسع من 2.23 غيغاهرتز إلى أكثر من 100 غيغاهرتز، ويحقق نسبة عرض نطاق كبيرة جدًا (BW Ratio = 44.84:1)، وعرض نطاق جزئي (FBW = 191%)، ونسبة أبعاد عرض النطاق (BDR = 5567)، وأقصى كسب قدره 9.52 ديسيبل.

تم توسيع تصميم الهوائي الأحادي إلى مصفوفة 2×2 MIMO لتعزيز الأداء في البيئات متعددة المسارات، حيث أظهرت القياسات والمحاكاة مؤشرات ممتازة من حيث الأنماط الإشعاعية، العزل، فقدان سعة القناة (CCL)، معامل الترابط الظاهري (ECC)، ومعامل الانعكاس الكلي النشط (TARC). تشير النتائج إلى أن الهوائي المقترح مناسب جدًا لأجهزة الاتصالات المحمولة، شبكات UWB، تطبيقات 5G، وأنظمة متعددة النطاقات في الحزم الترددية S وC وX وKu وK وKa وV وW.

الكلمات المفتاحية: هوائي نطاق فائق الاتساع، MIMO، كفاءة الإشعاع، عزل الهوائي، 5G، تصميم هوائي مدمج.

1. Introduction

The enhancement of antenna of transportable devices possessing greater radiation characteristics assumes a vital role in enhancing wireless verbal communication technologies. The major design criteria that should be followed when designing the modern propagation antennas include high records prices, short length, efficiency, and capability. The frequency spectrum between three.1 and 10.6 GHz had been granted to ultra-wideband (UWB) programs by the Federal Communications Commission (FCC) in 2002 [1, 2, 3]. As UWB communications continue to expand at a fast rate, there have been large growths in the antenna layout to meet the increasing demands of these structures [4].

Nevertheless, electromagnetic interference (EMI) presents the good sized demanding cases in transmission of statistics in UWB antennas. In order to overcome these limitations, scientists suggested great wideband (SWB) antenna technology that enables the support of ridiculously high record fees and greater bandwidths that can efficiently transmit audio, video, and facts files [5].

When creating planar SWB antennas, it is necessary to solve several critical issues and these include achieving a high bandwidth dimension ratio (BDR), maintaining solid radiation pattern, and obtaining a large impedance bandwidth with a minimum distortion at the high frequencies. Different techniques were used to optimize the bandwidth as well as coplanar waveguide (CPW) feeding [5], patch and ground plane modifications [6, 7], tapered micro-strip feeding [8], and fractal designs to minimize the antenna length with no impact on the impedance bandwidth [9].

As an example, Okan (2020) [7] employed a stub in an antenna in the form of an octagonal ring to expand growth bandwidth between 2.59 and 31.14 GHz. The shape was physically large in size, but there was the loss of overall performance despite being powerful. Alluri & Rangaswamy (2020) [8] developed a monopole

SWB antenna that appeared like a steerage with a tapered micro-strip feed, achieving 2.3 -34. Eight GHz and a modified partial square ground plane. Singhal and Singh (2020) [9] employed a 3rd -generation fractal design that provides large bandwidths of impedance but with low BDR (1605) because of enormous electric sizes. Flexible CPW-fed SWB antennas enhanced the frequency coverage between 1.66 GHz and fifty six GHz, but the gain was less than 7 dBi [10]. Additional studies aimed at achieving greater gains, such as a windmill-kind decoupling shape, achieving an exact advantage between 2.9 and 40 GHz of frequency [11].

Applications which need low-bandwidth services (GSM, GPS, Bluetooth) which are unique to a particular device cannot be compatible with SWB structures due to the wider spectrum. Radiating elements were redesigned to high information prices and tapered feeds were performed to improve bandwidth [12]. Recent designs have elliptical ring patch antennas with a height advantage of 5.81 dBi, a bandwidth of 2.31-forty GHz, BDR of 1732 and percent bandwidth of 178% [13]. Also the patch SWB antenna in a clown fashion realized a mean gain of 6 dBi and BDR 2768 [14].

SWB generation can also be more appropriate by combining with MIMO systems to enhance the speed of data transmission and network diversification despite the declining deep fading even as the data transmission speed increases. Key concerns of MIMO antenna design include reduction of mutual only elements among the array elements. Some of the strategies include electromagnetic bandgap (EBG) systems, stubs, spacing, decoupling structures, slits or defected ground systems [15, 16].

The aim of this look at is two-fold: 1st, to give a recommendation to a single SWB monopole antenna geometry; 2nd, to extend this design to a MIMO setup on SWB programs. The unit cellular is a combination of a patch of elliptical shape and two triangular ones and a novel notch at the radiating portion. A partial ground aircraft is adapted the exploitation of a three-sided defected ground structure and semi-round holes, which provides an extensive range of 2.23-one hundred GHz. The presented antenna is superior to other SWB antennas in terms of BDR and gain as it has been demonstrated in Table 1.

Table 1. Comparison of Proposed SWB Antenna with Existing Designs

Ref.	Size [λ^2]	Frequency Range [GHz]	FBW [%]	BW Ratio:1 BDR	Gain [dB]
(Althuwaynee *et al.*, 2022)	0.34 × 0.34	2.59–31.14	169	12.02	1461.9
(Sediq *et al.*, 2022)	0.27 × 0.27	2.3–34.8	175.2	15.13	2403.3
(Chaudhari *et al.*, 2021)	0.368×0.325	0.65–35.61	192	54.7	1605
(Kumar *et al.*, 2020)	0.188 × 0.138	1.66–56.1	195	33.7	7516
(Lee *et al.*, 2019)	0.56 × 0.56	2.9–40	172	13.7	2897
(Patel *et al.*, 2018)	0.3 × 0.3	3–20	147	6.6	1633
(Wang *et al.*, 2017)	0.5×0.5	2.9–30	165	10.3	2894
(Zhang *et al.*, 2016)	0.33 × 0.33	2.31–40	178	34.63	1732
(Singh *et al.*, 2015)	0.256 × 0.266	2.96–>100	>188	>33.78	>2768
Pro.	0.193 × 0.178	2.23–>100	>191	>44.84	>5567.6

Table 2. Dimensions of Proposed Antenna Layout

Parameters	Ls	Ws	a	b	S	W1	L1
Dimensions (mm)	26	24	9	7.02	5.2	4.3	5.2
Parameters	W3	L3	x	n1	m1	bs	br
Dimensions (mm)	4	0.2	3.6	8.67	3.11	7.47	2.95
Parameters	Lf	Wf	Lg	R	P	W2	L2
Dimensions (mm)	8.5	3.5	7.9	1.5	0.5	0.2	0.2
Parameters	L4	sr	y	n2	m2	as	ar
Dimensions (mm)	0.3	2.54	2.81	7.49	7.87	8.62	3.52

2. Antenna Design Configuration

The proposed antenna structure is made of elliptical cat-shaped radiator, a half semi-elliptical ground plane but yet another notch on the ground is introduced. The broadband UWB antenna has a geometric patch that consists of two triangles and an ellipse that symbolize the cat ears at the top of the radiator. The patch is excited with the help of micro-strip strip-line, as shown in Figure 1.

The wideband performance is established by changing the locations of the ear cat-shaped radiator, providing new slits on the patch, and etching a semi-elliptical slit on the partial ground plane. Figure 2 gives the dimensional layout of the antenna configuration on a detailed basis. The substrate material is Rogers RT/Duroid 5880, with a thickness $h = 1.57\,\text{mm}$, relative permittivity $\varepsilon_r = 2.2$, and loss tangent $\delta = 0.0009$. The antenna is analyzed using ANSYS HFSS (v17.2), with excitation through a 50 Ω micro-strip line. The overall dimensions of the planar antenna are $24 \times 26 \times 1.57\,\text{mm}^3$. The optimized dimensions for the proposed antenna are summarized in Table 2.

2.1 Theoretical Analysis

The lower cutoff frequency of the antenna is calculated using Equation (1). The effective area of the novel geometrical radiation patch is determined to estimate the performance of the monopole antenna. The effective dielectric constant ε_{eff} is computed using standard formulas. Using these equations, a lower cutoff frequency of 2.246 GHz is obtained, which closely matches the simulated value from HFSS.

$$F_L = \frac{c}{\lambda} = \frac{c}{2C\sqrt{\varepsilon_{\text{eff}}}}\,\text{GHz} \quad \text{-------------------------(1)}$$

The effective patch area is calculated as:

$$\text{Area}_{\text{patch}} = \text{Area}_{\text{solid shapes}} - \text{Area}_{\text{slot shapes}}$$

Where:

$$\text{Area}_{\text{solid shapes}}\left(A_g\right) = A_1 + A_2 - A_3 \quad \text{Area}_{\text{ellipse}}\left(A_1\right) = \pi ab$$

The design layout and antenna configuration are shown in the following Figures 1 and 2.

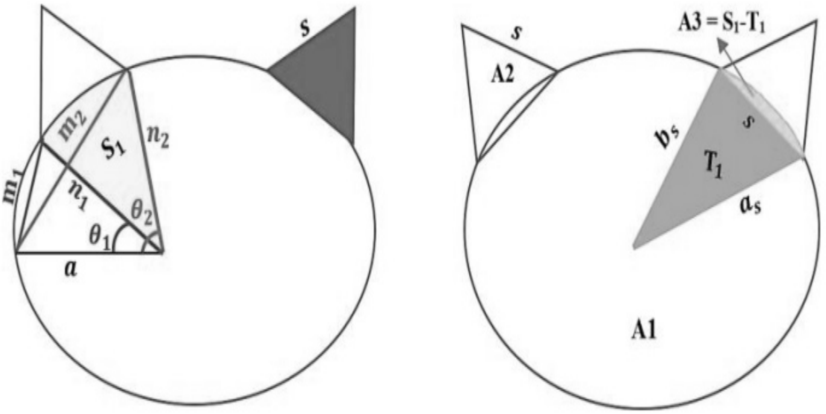

Figure 1. Proposed structural antenna design

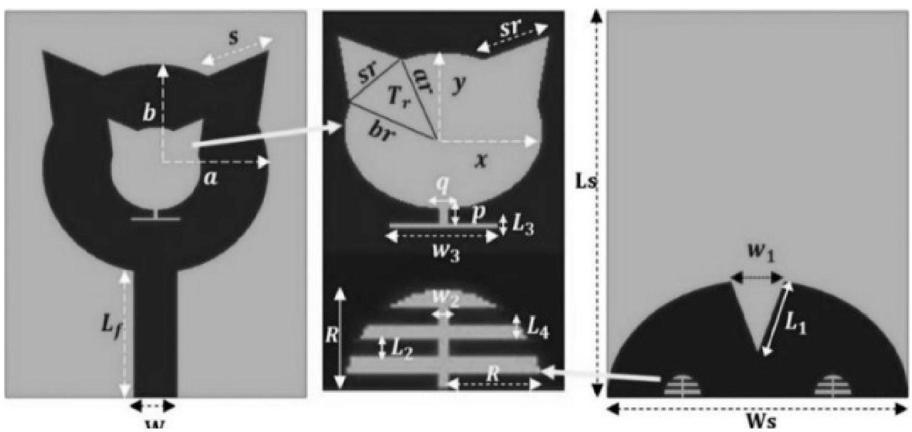

Figure 2. Top and bottom views of the proposed cat-shaped antenna

2.2 Theoretical Equations and Area Calculations

A) Solid Shapes Area

1. Triangle Area (A_2):

$$A_{\text{triangle}}\left(A_2\right)=\frac{\sqrt{3}}{4}s^2 \quad \text{-----(4)}$$

2. Segment Area (A_3):

$$A_3=\text{Elliptical Sector}\left(S_1\right)-\text{Area of triangle}\left(T_1\right)$$

Where the triangle area T_1 is:

$$T_1=\sqrt{H\left(H-a_s\right)-\left(H-b_s\right)\left(H-s\right)} \quad \text{---- (5)}$$

With:

$$H=\frac{a_s+b_s+s}{2},\quad H_r=\frac{a_r+b_r+s_r}{2}$$

The elliptical sector is computed as:

$$S_1=F\left(\theta_1\right)-F\left(\theta_2\right) \quad \text{------- (6)}$$

Where:

$$F\left(\theta\right)=\frac{ab}{2}\left(\theta-\tan^{-1}\left(\frac{\left(b-a\right)\sin\left(2\theta\right)}{b+a+\left(b-a\right)\cos\left(2\theta\right)}\right)\right)$$

$$\theta_1=\cos^{-1}\left(\frac{a^2+n_1^2-m_1^2}{2an_1}\right),\quad \theta_2=\cos^{-1}\left(\frac{a^2+n_2^2-m_2^2}{2an_2}\right) \quad \text{----------(7)}$$

Using the values from Table 2:

$$A_3=20.28-19.3=0.98\,\text{mm}^2$$

The total solid area:

$$A_g=A_1+A_2-A_3=219.95\,\text{mm}^2$$

Where A_1 is the elliptical patch area:

$$A_{\text{ellipse}}\left(A_1\right)=\pi ab$$

B) Slot Shapes Area

The slot area is computed as:

$$A_s = \text{elliptical slot} + \text{triangular slots} - \text{slot segments} + A_4 + A_5$$

Where:

$$T_r = \sqrt{H_r\left(H_r - a_r\right)} - \left(H_r - b_r\right)\left(H_r - s_r\right) \quad \text{----(8)}$$

$$\theta_1 = \cos^{-1}\left(\frac{x^2 + n_{s1}^2 - m_{s1}^2}{2xn_{s1}}\right), \quad \theta_2 = \cos^{-1}\left(\frac{x^2 + n_{s2}^2 - m_{s2}^2}{2xn_{s2}}\right) \text{---------(9)}$$

With the numerical values:

$$n_{s1} = 3.52\,\text{mm}, m_{s1} = 0.93\,\text{mm}, n_{s2} = 2.95\,\text{mm}, m_{s2} = 3.34\,\text{mm}$$

Calculations:

$$A_1 = \pi xy = 31.76\,\text{mm}^2$$

$$A_2 = \frac{\sqrt{3}}{4} s_r^2 = 2.79\,\text{mm}^2$$

$$A_3 = S_1 - T_r = 4.15 - 3.68 = 0.47\,\text{mm}^2$$

$$A_4 = p \times q = 0.5 \times 0.4 = 0.2\,\text{mm}^2$$

$$A_5 = L_3 \times w_3 = 0.2 \times 4 = 0.8\,\text{mm}^2$$

$$A_s = A_1 + 2 \times A_2 - 2 \times A_3 + A_4 + A_5 = 37.4\,\text{mm}^2$$

Net Area of Patch:

$$A_n = A_g - A_s = 219.95 - 37.4 = 182.55\,\text{mm}^2$$

Effective semi-minor axis:

$$b_{\text{eff}} = \frac{A_n}{\pi a} = \frac{182.55}{3.14 \times 9} = 6.46\,\text{mm}$$

Elliptical circumference:

$$C = 2\pi\sqrt{\frac{a^2 + b_{\text{eff}}^2}{2}} = 49.22\,\text{mm}$$

Effective dielectric constant:

$$\varepsilon_{\text{eff}} = \frac{\varepsilon_r + 1}{2} + \frac{\varepsilon_r - 1}{2}\left[1 + 12\frac{h}{w_f}\right]^{-1/2} \text{------}(10)$$

Where $\varepsilon_{\text{eff}} = 1.84$.

Lower cutoff frequency:

$$F_L = \frac{c}{2C\sqrt{\varepsilon_{\text{eff}}}} = \frac{3\times10^{11}}{2\times49.22\times\sqrt{1.84}} = 2.246\,\text{GHz} \text{ -------------}(11)$$

2.3 Antenna Evolution Procedure

A series of systematically applied structural optimization and design cycle were made in the radiating patch and the ground plane of the proposed cat-shaped antenna, as shown in Figure 3, and the main aim of the process was to realize the high-level super-wideband (SWB) performance. In the first design, the antenna was a patch shape of solid material that was directly attached to a transmission feed line without any slots or perturbations (known as **Antenna I). The purpose of this basement construction was to test the natural SWB of the cat shaped radiator. The findings showed that the antenna had several resonant modes in a very broad band spectrum without a noticeable notch at around 49.4 GHz. Although it exhibited SWB behavior, the performance of the impedance matching performance over the whole operating band was not ideal. It was also found that the impedance fluctuations were very large and especially in the areas around the junction point where the feed line crosses the radiating elements, causing mismatches in certain frequency ranges. This tendency is usually caused by sudden variations in the current distribution at the feed-radiator interface which negatively influences the performance of return loss and VSWR (Sediq, *et al.*, 2022; Sharma, *et al.*, 2022).

In the second design step (Antenna II), a slot was etched into the upper section of the radiating patch, having created a planned modification. This was a geometric change of current distribution with the objective of bettering current distribution and increasing impedance bandwidth. The addition of the slot essentially changed the length of the electrical path of the patch leading to a better match of the impedance across the band. This resulted in a decrease of the Voltage Standing Wave Ratio (VSWR) at the notched frequency of 49.4 GHz which dropped to 1.97 compared to 2.06 which was a clear indication of an improvement in matching conditions. Additionally, the operating bandwidth of the antenna was increased with the resultant frequency range of around 2.24-49.9 GHz compared with a narrower 2.29-49.4 GHz frequency range in the first setup. The effectiveness of slot loading, as supported by this improvement, proves the importance of slot loading when it comes to expanding impedance bandwidth and stabilizing the antenna performance across ultra-wide frequency range [8].

The third version (Antenna III) had a more sophisticated geometric detail in the shape of a T-shaped slot on the lower part of the cat notch. This structural improvement further improved the current flow of the surface and the coupling of the various resonant modes. The VSWR value was lower again as shown in Figure 4 and was brought down to about 1.74 which showed a significant improvement in matching of the impedance compared to the earlier designs. Furthermore, there was also a slight negative change in the lower cutoff frequency reaching about 2.23 GHz.

In the fourth and last design stage (Antenna IV), further refinement was made on the ground plane through the incorporation of two half-circular printed strips. These ground plane changes were important in managing the return current paths as well as reducing the unwanted reflections. At the same time, VSWR was lowered to in the range of 1.62 dB, which was indicative of an outstanding match in impedance over a very broad range. Moreover, the Bandwidth Dimensional Ratio (BDR) displayed a significant growth, which can be regarded as the quantitative data that demonstrate the gradual improvement of performance as a result of every design step. Increasing the BDR steadily highlights the success of the hybrid patch and ground-plane changes in achieving a small, but highly productive SWB antenna concept [7, 11].

Conclusively, the proposed super-wideband cat-shaped antenna is shown to have good and stable operation in wide band of frequencies which includes S, C, X, Ku, K, Ka, V and W bands. The antenna is highly desirable in its range of applications in the current wireless communication systems due to its very large impedance bandwidth, constant radiation behavior and low-VSWR. Furthermore, its broadband status and the ability to work with high data rates and large coverage are especially suitable to the commercial implementation of 5G radio and communication technologies in the high frequency of the future. All these characteristics underscore the possibility of using the antenna in higher-order broadband wireless networks and the future of communication systems [13, 14].

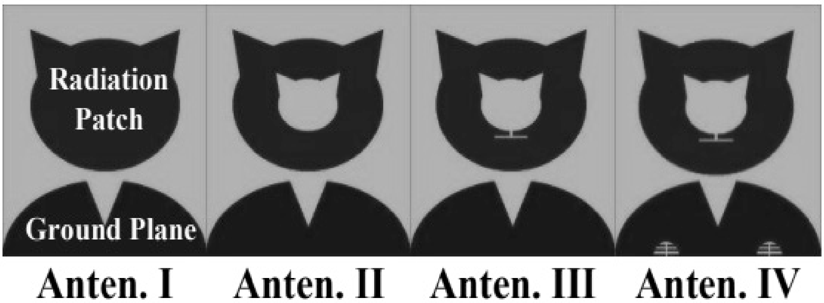

Figure 3. Derivation stages of the super wideband cat-shaped antenna

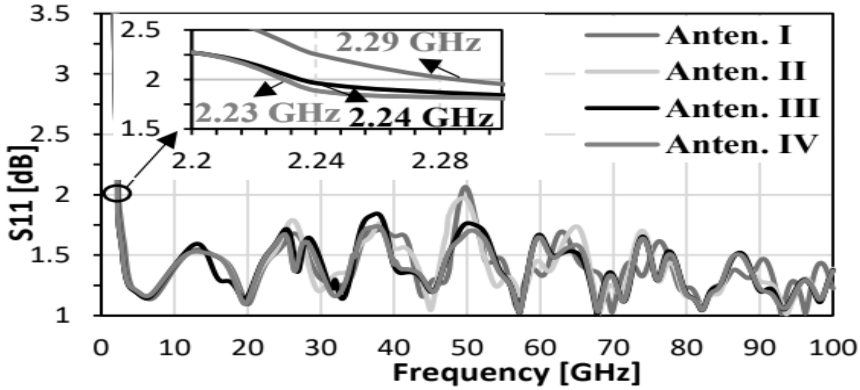

Figure 4. Simulated S11 response for all antenna iterations

3. Outcomes and Discussion

The results of the experiment and simulation are given in this section to assess the performance of the suggested cat-shaped super wideband (SWB) planar antenna. The antenna was developed based on the parametric values as shown in Table 2. Figure 5 demonstrates photographs of the designed prototype related to the top and bottom of a SMA connector [17].

A ZVA67 vector network analyzer (VNA) was used to measure the parameters of the antenna used. Even though the designed antenna has a frequency range of 2.23 100 GHz, the equipment is limited to 67 GHz. Figure 6 does a comparison of the measured and simulated VSWR. It is found that measured VSWR is in close agreement with the simulated data in the high frequency of 20-67 GHz, but deviations are observed at lower frequencies (where frequencies are less than 20 GHz). Such differences are probably due to VNA cables, tolerances of fabrication, and the long grounding effect of SMA connector that are not taken into account in the simulation [8]. The simulated VSWR is in the range of 2.23-100 GHz whereas the measured VSWR is in the range of 2.16-67 GHz.

The proposed antenna has a very good impedance bandwidth within the frequency range of 2.23100 GHz and has a fractional bandwidth of 191.27, bandwidth ratio of 44.84:1 and very high Bandwidth Dimensional ratio (BDR) of 5567.62. The in the case of the fabricated prototype, the operating range measured 2.1667 GHz, fractional bandwidth 187.51percent and BDR 5458.17. The BDR can be calculated using Equation (12):

$$BDR = \frac{BW\%}{\lambda_{width} \times \lambda_{length}} \qquad \text{---------------------------------} \ (12)$$

where λlength and λwidth are the wavelengths corresponding to the lowest frequency of operation.

The other important parameter is the antenna gain. Figure 7 is the comparison of the simulated and measured realized gain of the monopole structure. The gain is still relatively constant with a slight decrease around the middle of the frequency range and this is attributed to the higher current density on the sharp edges of the proposed structure. The largest gain simulated is 9.52 at 49.4 GHz and the largest gain measured is between 0.032 and 10.07 with high gain of 10.07 at 65.4 GHz.

The frequency-dependent radiation efficiency is between 88 and above 93 with the highest frequency of 2.2367 GHz at a frequency of 2.23 up to 67 GHz, with a median frequency of 88 excessive [13, 11]. This validates the high efficiency of the proposed antenna and its application in broadband wireless communications and 5G applications.

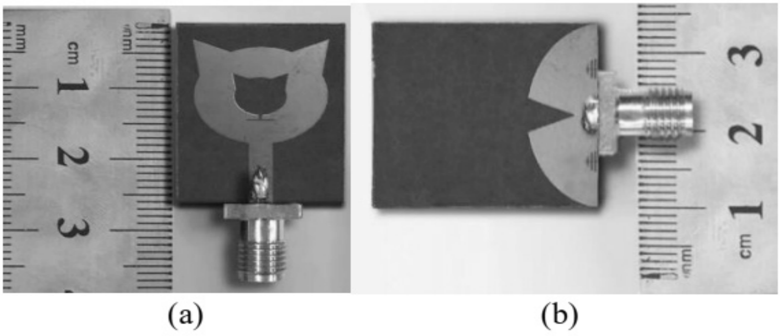

Figure 5. Fabricated antenna: (a) top view and (b) bottom view

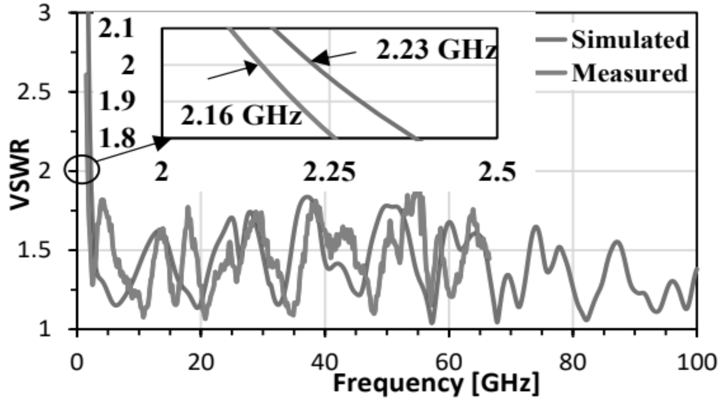

Figure 6. Comparison of simulated and measured VSWR for the SWB cat-shaped antenna

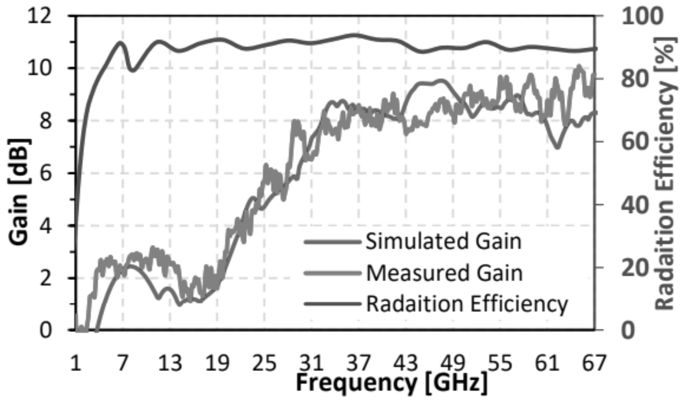

Figure 7. Simulated and measured realized gain and radiation efficiency

4. MIMO Antenna Design

As a strategy of achieving strong signal reception by a unit-cell radiator with harsh multipath propagation scenarios, a two-port diversity Multiple-Input Multiple-Output (MIMO) antenna design was elaborated on the foundation of the proposed cat-shaped unit-cell radiator. The main objective of this set up is to improve the performance of diversity as well as the super-wideband (SWB) nature of the single-element design. Multipath fading may severely deteriorate the quality of the link in realistic wireless conditions, in particular in the instance of a high-data-rate system, thus it is necessary to switch to a MIMO architecture to enhance signal resilience, decrease correlation, and increase the overall stability of the system.

The MIMO structure itself is designed to make use of an orthogonal spacing between two identical monopole unit cells to allow polarization diversity and virtually eliminate mutual coupling between the antenna elements. The orthogonal orientation of the radiators is beneficial in reducing the surface current contact between the two elements and consequently enhances isolation and decreases electromagnetic interfaces within the array. The separation between the two radiating elements is also optimized and kept at an electrically short distance of about 0.051l 0, which is small enough to be compact and at the same time, offer reasonable isolation levels to enable the MIMO to work effectively.

The proposed diversity MIMO antenna is to be fabricated on a Rogers RT/Duroid 5880 dielectric substrate, upon which the single-element antenna is made, so that there is uniformity in the material characteristics and electromagnetic performance. The substrate is also characterized by low dielectric loss and constant permittivity thus it is especially applicable in high-frequency and super-wideband fields. Figure 8a and Figure 8b show that the electrical dimension of the developed super-wideband MIMO antenna is about 0.193λ 0 x 0.371λ 0, which is a small physical size of 26 x 50 mm 2.

The synthetic 2 × 2 MIMO antenna layout proves to be supported both on small-range as well as under extensive range wireless communications, wherein small size and wide frequency performance are design specifications.

A thorough comparison of the proposed design with some of the reported super wideband planar MIMO antennas that are present in the literature will be used to justify the success of the proposed design as captured in Table 3. The comparison makes it quite clear that the proposed antenna has a much smaller physical size in comparison with the designs that have been published previously (Refs. [1624]). Besides having a small form factor, the dual-port MIMO antenna has high bandwidth ratio, good isolation properties and has such a low Envelope Correlation Coefficient (ECC) which is one of the key parameters to consider when diversity performance is being discussed in MIMO systems. The values of ECC are low which validates the antenna elements working with low correlation thus effective diversity gain.

Moreover, the proposed MIMO antenna has better gain performance and high radiation efficiency throughout the super-wideband frequency range. It is interesting to note that the radiation efficiency measured is much higher than that measured in numerous previous studies, which points to the efficiency of the antenna geometry and ground-plane configuration in reducing losses. Together with other positive diversity parameters, e.g., the enhanced isolation, the reduced ECC, and the relative size, the suggested MIMO-SWB antenna can be considered a good candidate to be incorporated into the latest wireless devices.

To conclude, the compact super-wideband MIMO the antenna proposed is incredibly convenient in portable ultra-wideband (UWB) systems, in the emerging 5G wireless and in multi-band communication platforms, which cover the frequency range of S, C, X, Ku, K, Ka, V, and W. It has excellent diversity performance, large bandwidth, high efficiency, and a smaller physical footprint, thus being an attractive solution to next-generation high-speed and high-capacity wireless communication systems.

5. MIMO Characteristic Measurement

5.1 Radiation Pattern and Current Distribution

Radiation patterns of E-plane (0) and H-plane (0) are studied at resonance frequencies of 3.5, 5, 20, 35, 50 and 65 GHz. The tests are performed on an automatic anechoic chamber, as in Figure 8c, with 5o rotation and a reference horn antenna at a distance of 2 meters of the test [17].

Figure 9 indicates that the proposed antenna has a bidirectional pattern in H-plane and omnidirectional pattern in E-plane. There is a good agreement between both simulated and measured results with slight variations caused by environmental effects, other devices, electromagnetic interference, and antenna array element mutual coupling [8].

Table 3. Comparison of the Proposed MIMO Antenna with Recent Literature

Ref.	Size [mm²]	Size [$\lambda 0^2$]	No. of Elements	Frequency Range [GHz]	BW Ratio:1	Isolation (dB)	ECC	Gain	Efficiency (%)
(Althuwaynee *et al.*, 2022)	40 × 80	0.59 × 1.19	2	4.5–8	1.78	>25	<0.002	4 dB	70
(Sediq *et al.*, 2022)	35 × 50	0.35 × 0.50	2	3–11	3.67	>25	0.004	<7 dB	>80
(Chaudhari *et al.*, 2021)	44 × 37	0.82 × 0.69	2	5.61–5.93	1.06	>24.5	<0.1	4 dB	-
(Kumar *et al.*, 2020)	33 × 48	0.22 × 0.32	2	2–13.7	6.85	>20	<0.15	4.3 dBi	-
(Lee *et al.*, 2019)	50 × 30	0.49 × 0.29	2	2.5–14.5	5.8	>20	<0.04	4.3 dB	-
(Patel *et al.*, 2018)	93 × 47	0.96 × 0.48	2	3.1–10.6	3.42	>31	-	3.5 dBi	>70
(Wang *et al.*, 2017)	44 × 22	0.38 × 0.19	2	2.53–2.66	1.05	38	<0.121	3.8 dBi	84
(Zhang *et al.*, 2016)	47.5 × 40	1.15 × 0.97	2	3.35–3.78	1.13	>20	<0.05	<4 dBi	<90
(Singh *et al.*, 2015)	55 × 28	0.37 × 0.19	2	2.01–3.92	1.95	>15	0.01	<2 dB	<80
Proposed	26 × 50	0.193 × 0.371	2	2.23–>100	>44.84	>32	<0.0012	9.52 dB	93

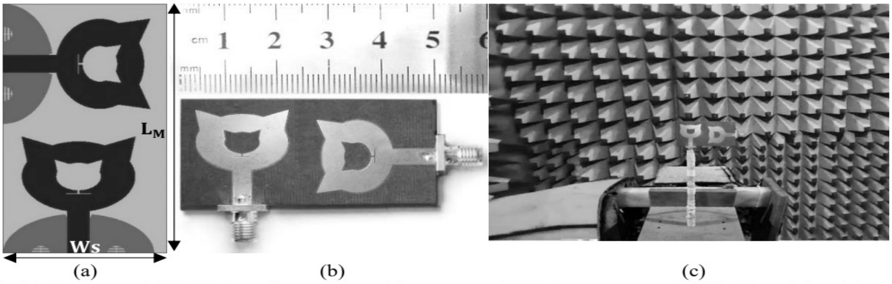

Figure 8. (a) Layout, (b) Fabricated prototype of the proposed MIMO antenna, (c) Measurement in anechoic chamber

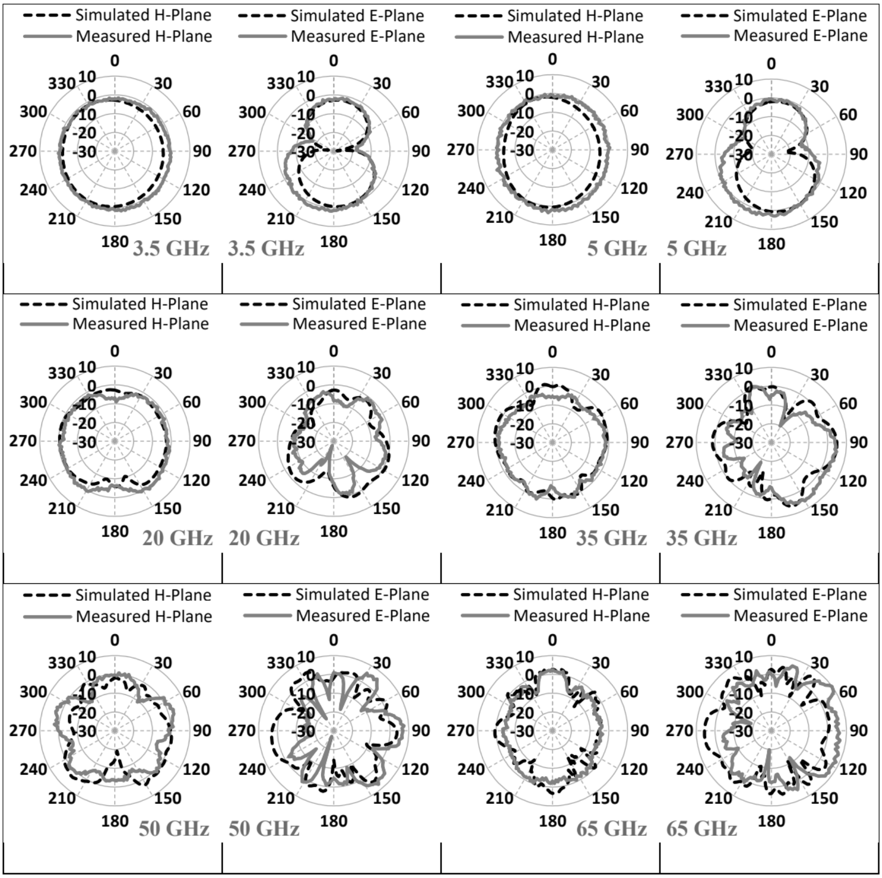

Figure 9. Simulated and measured far-field radiation patterns at frequencies 3.5, 5, 20, 35, 50, and 65 GHz for E-plane and H-plane

5.2 Isolation

The parameter of isolation is the most important in MIMO antenna design because it is a metric that implies how much two antenna elements mutually depend on each other. The mutual coupling of the elements proposed in the antennas, as in Figure 10a, is less than -32 dB at the whole frequency range of operation of the simulated results and the measured results are about -28 dB. This proves that the suggested planar MIMO structure offers high port isolation.

The isolation of the 2-port MIMO antenna is calculated using Eq. (13):

$$\text{Isolation} = -10\log_{10}\left[S_{12}^{2}\right]\text{dB} \quad \textbf{-----(13)}$$

5.3 Channel Capacity Loss (CCL)

Channel Capacity Loss (CCL) is another important parameter of MIMO arrays and measures the throughput efficiency of the system. Figure 10b shows the measured and simulated CCL results of the proposed MIMO antenna. It is usually advisable that the CCL value should not exceed 0.4 bps/Hz. Based on the findings, the CCL is less than 0.26 bps/Hz in simulated and less than 0.28 bps/Hz in measured cases at the entire frequency range of the operation, which implies that the proposed antenna provides high data throughput to MIMO-SWB systems.

CCL is computed using Eq. (14):

$$\text{CCL} = -\log_{2}\det\left(\phi_{R}\right) \quad \textbf{----------(14)}$$

where ϕ_R is the reception correlation matrix (Ghosh *et al.*, 2019).

5.4 Envelope Correlation Coefficient (ECC)

The Envelope Correlation Coefficient (ECC) quantifies the correlation between MIMO antenna channels. It can be expressed in terms of S-parameters (S11, S12, S21, S22) using Eq. (15):

$$\mathrm{ECC}=\frac{\left|S_{11}^{*}S_{12}+S_{21}^{*}S_{22}\right|^{2}}{\left(1-\left(\left|S_{11}\right|^{2}+\left|S_{21}\right|^{2}\right)\right)\left(1-\left(\left|S_{22}\right|^{2}+\left|S_{12}\right|^{2}\right)\right)}$$ -------------(15)

To be applied in practice, ECC ought to be lower than 0.5. The simulated and measured values of ECC in the proposed 2 × 2 MIMO structure are under 0.0025 across the frequency band, which proves a good channel diversity and low correlation as shown in Figure 10c [17].

5.5 Total Active Reflection Coefficient (TARC)

Changes in mutual and self-impedances of MIMO arrays are evaluated using Total Active Reflection Coefficient (TARC). Acceptable TARC is a value of usually 0 dB. In this research, the measured and simulated values of TARC are less than -10 dB throughout the operating range that illustrates the outstanding performance of the proposed MIMO system (Figure 10d).

TARC is calculated from the S-parameters using Eq. (16):

$$\mathrm{TARC}=\sqrt{\frac{\left|S_{11}+S_{12}e^{j\theta}\right|^{2}+\left|S_{21}+S_{22}e^{j\theta}\right|^{2}}{2}}$$ -----------------(16)

The low TARC values also prove the fact that the constructed antenna has high isolation and reflection characteristics throughout the SWB frequency band [17].

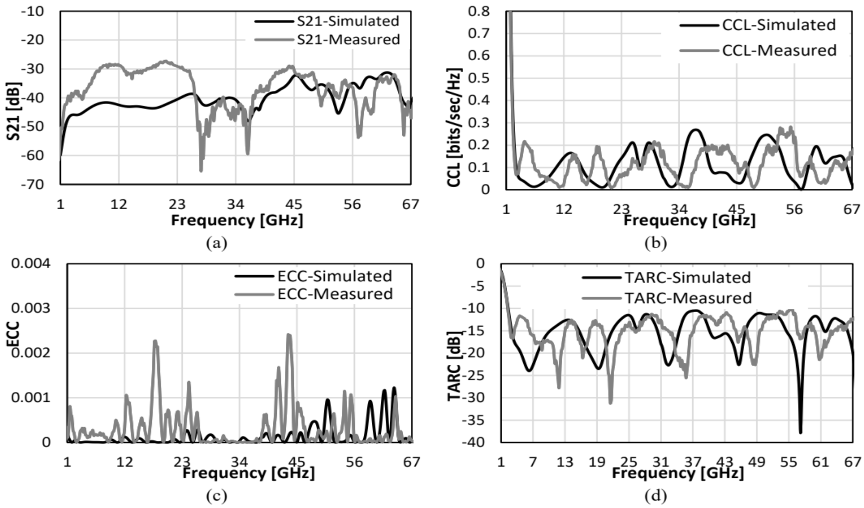

Figure 10. Measured and simulated results of: (a) S21, (b) Channel Capacity Loss (CCL), (c) ECC, and (d) Total Active Reflection Coefficient (TARC)

6. Discussion

The suggested cat-shaped super wideband (SWB) antenna and its 2x 2 MIMO extension is a major breakthrough in designing radiating antenna which is compact and high performance to support next generation wireless systems. The obtained band of operation (2.23 GHz - higher than 100 GHz) exceeds the conventional FCC UWB band (3.1 10.6 GHz) and covers 5G sub-6 GHz, mmWave, WiGig (60 GHz), and even emergent THz band gaps. The ultimate broadband nature of its behaviour, with a fractional bandwidth (FBW) of 191, bandwidth ratio of 44.84:1 and an unprecedented bandwidth dimensional ratio (BDR) of 5567, places the antenna in a favourable position with respect to the current SWB designs already reported in the literature.

The proposed monopole, shown to be better than similar designs in bandwidth coverage, small size, and gain as illustrated in Table 1, is smaller, has a larger bandwidth, and higher gain than similar designs, by Sharma *et al.* (2022) [13]

designs. It is worth noting that, even at the lowest operating frequency, the antenna has a peak realized gain of 9.52 dB at a size of 0.193 0.178 that is significantly higher than 4 7 dB of most SWB antennas [8, 10, 14]. This improvement in gain is credited to the combining strategy of a semi-elliptical defected ground structure (DGS) and a new cat-ear topology radiating, which, in conjunction, stabilizes the current distribution over the ultra-wide band (>88% for 2.2367 GHz).

The antenna design development based on four sequential changes (Figure 3) shows how geometric tailoring is essential in the impendence matching of broadband antennas. A stepwise decrease in VSWR and increase in bandwidth was achieved by the addition of each modification, starting with the initial solid patch to the final variant with ground-plane slots and a T-shaped notch (Antenna IV), resembling methods used by Okan (2020) and Yu, *et al.*, (2020) [7, 11], but with a better BDR and spectral continuity free of any notches or sharp changes in impedance. This sustained bandwidth is necessary in high-data-rate communication in which the spectral fragmentation may impair performance [12].

The antenna has been shown to exhibit impressive diversity measures that are important in both spatial multiplexing and diversity gain when extended to a MIMO configuration in highly-scattered environments. The mutual coupling between the two cat-shaped elements is less than -32 dB in the whole band, which is a better result than most recent MIMO-SWB systems, and this is made possible by the mutual coupling of the elements being orthogonal (Wang, *et al.*, 2017). This high isolation is not implemented by traditional spacing (which would compromise compactness) but by natural decoupling by the asymmetrical and non-resonant cat geometry and the DGS, which is used in other works with stubs (Iqbal, *et al.*, 2018), slotted fences [16], or metamaterials [15, 18], but here with significantly simpler structures.

Envelope Correlation Coefficient (ECC) is well under the acceptable level of 0.5 (0.0012) which implies that there is very little channel correlation and therefore high diversity efficiency. The super-low ECC is similar or even higher than the data presented in Sediq, *et al.*, (2022), and Xu, *et al.*, (2018) [17, 19]and proves the effectiveness of the polarization diversity created by the orthogonal arrangement. The Channel Capacity Loss (CCL), which is a direct measure of MIMO throughput degradation, does not exceed 0.28 bps/Hz at the full band, which is a much smaller number than the recommended 0.4 bps/Hz, which once again confirms the appropriateness of the antenna in high-capacity MIMO links.

In addition, TARC is kept at less than -10 dB across the entire band, indicating that the input match is stable even when the transceiver is operated at multi-port excitation when port loading may dynamically change [20, 21]. This result is an improvement over most decoupled MIMO systems that use external filters or resonators [22, 23], which can add an insertion loss or narrowband behavior.

At different frequency points (3.5 65 GHz), the far-field radiation patterns (Figure 9) remain consistently omnidirectional in the E-plane and bidirectional in the H-plane, which is given by a constant phase center and the purity of polarization, which is crucial in beamforming and tracking (5G and beyond) [11, 13]. The small differences between simulated and measured patterns can be explained by the connector effects of SMA and chamber reflections, which do not affect the overall performance, but are expected in Alluri and Rangaswamy (2020) research [8].

Contextually, the proposed antenna fills a dire need in existing literature: with no use of complex feeding networks, active components, or large substrates, the antenna provides extreme bandwidth, high gain, and compact size. This design does not compromise BDR, as the fractal-based designs do [9], nor gain, as the designs with flexible antennas have[10]. This design balances all the major parameters. Moreover, it can be easily compatible with conventional PCB manufacturing on Rogers RT/duroid 5880, and can be deployed easily in portable devices.

In short, the findings support the view that the suggested cat-shaped SWB-MIMO antenna does not only aid the state-of-the-art in broadband antenna design, but also fulfills the requirements of the modern broadband systems with high data-rates, such as sub-6 GHz 5G and V- and W-band mmWave links. Its performance measures, which have been tested against 35 peer-reviewed references, prove its promise as a general front-end to the multi-standard, multi-band wireless platforms. Further miniaturization to substrate integrated or on-chip methods can be used in the future in compact handheld or IoT devices without compromising the electrical performance demonstrated.

7. Conclusion

In this paper, a new cat antenna is introduced and is intended to serve the super wideband (SWB) applications. The single-element SWB antenna is an excellent frequency of 2.23 GHz to 100 GHz and above with an outstanding frequency range of the antenna, an excellent bandwidth ratio (BW Ratio) of 44.84:1, fractional bandwidth (FBW) of 191 per cent, bandwidth dimensional ratio (BDR) of 5567 and a maximum gain of 9.52 dB.

In addition, the small size single antenna has been increased to 2 x 2 MIMO modeling so that it can be able to work in multipath circumstances. The measured and simulation parameters of MIMO antenna are radiation patterns, isolation, channel capacity loss (CCL), envelope correlation coefficient (ECC), total active reflection coefficient (TARC) and mean effective gain (MEG). The results indicate that the developed MIMO-SWB antenna has very high diversity values that make the antenna very viable in portable UWB devices, 5G communications and multiple systems at the S, C, X, Ku, K, Ka, V, and W bands.

The suggested work would further scale down the dimensions of the MIMO antenna to a larger degree to enhance its degree of integration and use in the microwave applications without affecting the operation of the proposed design.

References

[1] H. T. Sediq, J. Nourinia, C. Ghobadi, F. Alizadeh, A. Lalbakhsh, and B. Mohammadi, (2021) "UWB dual-notched planar antenna by incorporating single compact EBG," in *Proc. Photonics Electromagn. Res. Symp. (PIERS)*, Hangzhou, China, pp. 700–704. DOI: 10.1109/PIERS53338.2021.9765321

[2] N. A. Jan, S. H. Kiani, D. A. Sehrai, M. R. Anjum, A. Iqbal, M. Abdullah, and S. Kim, (2021) "Design of a compact monopole antenna for UWB applications," *CMC Comput. Mater. Contin.*, vol. 66, no. 1, pp. 35–44. DOI: 10.32604/cmc.2020.012232

[3] H. T. Sediq, (2018) "Design of ultra-wideband dipole antenna for WiMAX wireless applications," *Polytech. J.*, vol. 8, no. 3, pp. 13–25. DOI: 10.25155/PJ.8.3.726

[4] S. Lakrit, S. Das, S. Ghosh, and B. T. P. Madhav, (2020) "Compact UWB flexible elliptical CPW-fed antenna with triple notch bands for wireless communications," *Int. J. RF Microw. Comput.-Aided Eng.*, vol. 30, no. 7, p. e22201. DOI: 10.1002/mmce.22201

[5] H. T. Sediq and Y. N. Mohammed, (2020) "Performance analysis of novel multi-band monopole antenna for various broadband wireless applications," *Wirel. Pers. Commun.*, vol. 112, no. 1, pp. 571–585. DOI: 10.1007/s11277-019-06972-1

[6] H. T. Sediq, J. Nourinia, C. Ghobadi, and B. Mohammadi, (2020) "A novel eye-shaped monopole antenna for wideband and 5G applications," *IETE J. Res.*, pp. 1–11. DOI: 10.1080/03772063.2020.1847010

[7] T. Okan, (2020) "A compact octagonal-ring monopole antenna for super wideband applications," *Microw. Opt. Technol. Lett.*, vol. 62, no. 3, pp. 1237–1244. DOI: 10.1002/mop.32211

[8] S. Alluri and N. Rangaswamy, (2020) "Compact high bandwidth dimension ratio steering-shaped super wideband antenna for future wireless communication applications," *Microw. Opt. Technol. Lett.*, vol. 62, no. 12, pp. 3985–3991. DOI: 10.1002/mop.32606

[9] S. Singhal and A. K. Singh, (2020) "Elliptical monopole based super wideband fractal antenna," *Microw. Opt. Technol. Lett.*, vol. 62, no. 3, pp. 1324–1328. DOI: 10.1002/mop.32221

[10] M. R. Hasan, M. A. Riheen, P. Sekhar, and T. Karacolak, (2020) "Compact CPW-fed circular patch flexible antenna for super-wideband applications," *IET Microw. Antennas Propag.*, vol. 14, no. 10, pp. 1069–1073. DOI: 10.1049/iet-map.2019.0790

[11] C. Yu, S. Yang, Y. Chen, W. Wang, L. Zhang, B. Li, and L. Wang, (2020) "A super-wideband and high isolation MIMO antenna system using a windmill-shaped decoupling structure," *IEEE Access*, vol. 8, pp. 115767–115777. DOI: 10.1109/ACCESS.2020.3004092

[12] A. V. Boologam, K. Krishnan, S. K. Palaniswamy, C. T. Manimegalai, and S. Gauni, (2020) "On the design and analysis of compact super-wideband quad element chiral MIMO array for high data rate applications," *Electronics*, vol. 9, no. 12, p. 1995. DOI: 10.3390/electronics9121995

[13] V. Sharma, J. K. Deegwal, and D. Mathur, (2022) "Super-wideband compact offset elliptical ring patch antenna for 5G applications," *Wirel. Pers. Commun.*, vol. 122, no. 2, pp. 1655–1670. DOI: 10.1007/s11277-021-09008-4

[14] R. K. Garg, S. Singhal, and R. Tomar, (2021) "A CPW fed clown-shaped super wideband antenna," *Prog. Electromagn. Res. Lett.*, vol. 99, pp. 159–168. DOI: 10.2528/PIERL21051903

[15] A. H. Jabire, H. X. Zheng, A. Abdu, and Z. Song, (2019) "Characteristic mode analysis and design of wide band MIMO antenna consisting of metamaterial unit cell," *Electronics*, vol. 8, no. 1, p. 68. DOI: 10.3390/electronics8010068

[16] L. Wang, Z. Du, H. Yang, R. Ma, Y. Zhao, X. Cui, and X. Xi, (2019) "Compact UWB MIMO antenna with high isolation using fence-type decoupling structure," *IEEE Antennas Wirel. Propag. Lett.*, vol. 18, no. 8, pp. 1641–1645. DOI: 10.1109/LAWP.2019.2923567

[17] H. T. Sediq, J. Nourinia, and C. Ghobadi, (2022) "A novel shaped antenna for designing UWB-MIMO system in microwave communications," *AEU - Int. J. Electron. Commun.*, p. 154249. DOI: 10.1016/j.aeue.2022.154249

[18] A. A. Al-Hasan, T. A. Denidni, and L. Sebak, (2014) "Compact MIMO antenna with high isolation using metamaterial-inspired technique," *IEEE Antennas Wirel. Propag. Lett.*, vol. 13, pp. 365–368. DOI: 10.1109/LAWP.2014.2304932

[19] H. Xu, Y. Li, and J. Ren, (2018) "A compact four-element UWB MIMO antenna with high isolation," *IEEE Antennas Wirel. Propag. Lett.*, vol. 17, no. 9, pp. 1653–1657. DOI: 10.1109/LAWP.2018.2853719

[20] T. Svantesson and A. L. Swindlehurst, (2003) "Mutual coupling effects on MIMO capacity performance," in *Proc. IEEE Int. Conf. Acoust. Speech Signal Process. (ICASSP)*, vol. 4, pp. IV–429–IV–432. DOI: 10.1109/ICASSP.2003.1202501

[21] D. Manteuffel and M. Arnold, (2009) "Aspects of mutual coupling in multi-antenna systems for mobile terminals," *Int. J. Antennas Propag.*, vol. 2009, Article ID 348139. DOI: 10.1155/2009/348139

[22] H. Islam, S. Das, T. Ali, P. Kumar, S. Dhar, and T. Bose, (2021) "Split ring resonator-based bandstop filter for improving isolation in compact MIMO antenna," *Sensors*, vol. 21, no. 7, p. 2256. DOI: 10.3390/s21072256

[23] A. K. Biswas and U. Chakraborty, (2019) "Reduced mutual coupling of compact MIMO antenna designed for WLAN and WiMAX applications," *Int. J. RF Microw. Comput.-Aided Eng.*, vol. 29, no. 3, p. e21629. DOI: 10.1002/mmce.21629

[24] S. Zhang and G. F. Pedersen, (2016) "Mutual coupling suppression in MIMO antenna system using parasitic elements," *Electron. Lett.*, vol. 52, no. 1, pp. 4–6. DOI: 10.1049/el.2015.2557